Small-angle x-ray scattering study of the aggregation of gold nanoparticles during formation at the toluene-water interface

M. K. Bera,[1,2] M. K. Sanyal,[1,3] L. Yang,[4] K. Biswas,[3,5] A. Gibaud,[6] and C. N. R. Rao[3,5]
[1]*Surface Physics Division, Saha Institute of Nuclear Physics, 1/AF, Bidhannagar, Kolkata 700064, India*
[2]*S. N. Bose National Centre for Basic Sciences, JD-Block, Sec-3, Salt Lake, Kolkata 700098, India*
[3]*International Center for Materials Science, Jawaharlal Nehru Center for Advanced Scientific Research, Jakkur P.O., Bangalore 560064, India*
[4]*National Synchrotron Light Source, Brookhaven National Laboratory, Upton, New York 11973-5000, USA*
[5]*Solid State and Structural Chemistry Unit, Indian Institute of Science, Bangalore 560012, India*
[6]*LPEC, Universitá du Maine, UMR 6087 CNRS, Avenue O. Messiaen, 72085 Le Mans, France*
(Received 15 May 2009; revised manuscript received 28 January 2010; published 10 March 2010)

We report the results of an *in situ* small-angle x-ray scattering (SAXS) study of the aggregation of gold nanoparticles formed by an interfacial reaction at the toluene-water interface. The SAXS data provide a direct evidence for aggregate formation of nanoparticles having 1.3 nm gold core and an organic shell that gives a core-core separation of about 2.5 nm. Furthermore, the nanoparticles do not occupy all the cites of 13-member cluster. This occupancy decreases with reaction time and indicate reorganization of the clusters that generates planner disklike structures. A gradual increase in fractal dimension from 1.82 to 2.05 also indicate compactification of cluster aggregation with reaction time, the final exponent being close to 2 expected for disklike aggregates.

DOI: 10.1103/PhysRevB.81.115415 PACS number(s): 61.05.cf, 61.43.Hv, 61.46.Bc

I. INTRODUCTION

Nanoparticles of gold exhibit unique electrical,[1,2] magnetic,[3–5] optical,[1,6,7] and catalytic[8,9] properties. For instance, 55-atom gold nanoparticles of ~1.2 nm diameter supported on inert materials are found[9] to act as catalysts for the selective oxidation of styrene by oxygen. In another study,[8] it has been shown that gold nanoparticles can act as tunable active catalysts for the oxidation of alkenes with air exhibiting exceptionally high selectivity and conversions. Presence of ferromagnetism in gold nanoparticles has been established by magnetic measurements.[4,5] The catalytic and magnetic properties exhibited by gold nanoparticles with size below 2 nm, are of great importance.

Many methods have been developed[10–12] to prepare gold nanoparticles but the formation of monodispersed gold nanoparticles of size below 2 nm has not been understood. X-ray scattering[13] and atomic force microscopy measurements[14] have shown the formation of 13-member cluster of 1.2 nm gold nanoparticles by a liquid-liquid interfacial reaction.[11,12] Besides the size of the gold core of the nanoparticles, it has not been possible to measure the core-core separation directly. Thus, the nature of the aggregation process of the gold-core-organic-shell nanoparticles at the toluene-water interface is far from being clear, particularly in the case of thick films.

In this paper, we present the results of a small-angle x-ray scattering (SAXS) study that directly provide the size of the gold core of the nanoparticles and core-core separation that arises due to the presence of the organic shells. The SAXS measurements also allow us to probe the aggregation process of the nanoparticles at the toluene-water interface. Interestingly, the results presented here show that one can get almost monodispersed gold nanoparticles even when the interfacial film becomes[14] thick in the absence of an antivibration table. The use of an antivibration table slows down the reaction drastically and does not permit the large-scale production of the core-shell nanoparticles. Fluctuations, microscopic as well as macroscopic, at the liquid-liquid interface play a crucial role in interfacial reactions.[15] The formation of 1.2 nm nanoparticles at the interface is attributed[13] to 1 nm fingerlike microscopic fluctuations[15] at the toluene-water interface during the reaction. The macroscopic fluctuations at the interface, introduced by external mechanical vibrations in the absence of the antivibration isolation, can increase the rate of the reaction to form thicker films.[14] The present results show that the size of the gold core remain almost unchanged even as the film became thick.

SAXS is an established technique[16–22] to probe aggregation processes and this technique has been extended to grazing-incidence geometry [known as grazing-incidence small-angle x-ray scattering (GISAXS)] to make it sensitive for surface/interface studies. We have used this technique here to understand aggregation process at the liquid-liquid interface. The two-dimensional nature of the liquid-liquid interface makes the SAXS measurement and its analysis more challenging. Scattering in typical SAXS measurements is three dimensional in nature wherein a confined beam of x ray is allowed to scatter from a sample of interest and the scattered intensity is measured as a function of wave-transfer vector $\vec{q}(q_x,q_y,q_z)$. In GISAXS measurements, the incident angle is kept at a small angle, around the critical angle of the interface and the scattering becomes different in q_z and q_x (or q_y) directions. In the present experiment, two-dimensional scattering is obtained in the initial stage of reaction but as the amount of nanoparticles increases at the interface due to reaction and the film thickens, the scattering tends to become isotropic in all the directions and depends only on the magnitude of the wave vector, i.e., $q=|\vec{q}|=\sqrt{q_x^2+q_y^2+q_z^2}$. We shall discuss experimental details in the next section. In the subsequent sections, data analysis and results will be discussed.

II. EXPERIMENTAL DETAILS

A. Details of the reactions

In the present study, we have used low concentrations of the chemicals compared to those used earlier[11] to slow down the reaction. We prepared fresh solutions of the gold precursor, $Au(PPh_3)Cl$ (triphenylphosphine gold chloride), in toluene, an aqueous solution of NaOH (sodium hydroxide) and THPC (tetrakis-hydroxymethyl phosphonium chloride) of concentrations 0.25 mM (milli Molar), 0.625 mM, and 50 mM, respectively. THPC is the reducing agent in this reaction. We carried out the reactions in a specially prepared teflon cell kept on the goniometer table of beamline without vibration isolation (discussed in details in the next subsection). For the reactions, 2 ml solution of the gold precursor $Au(PPh_3)Cl$ in toluene was allowed to stand on 3 ml NaOH aqueous solution. The reaction was initiated by injecting 55 μl of THPC in the aqueous layer by a syringe with least disturbance of the interface. The injecting time of the reducing agent was taken to be the starting time of the reactions.

B. Experimental details

Absorption of x rays plays a crucial role in designing the geometry of SAXS measurements from a liquid-liquid interface. In conventional SAXS measurements, x rays are allowed to scatter from a dilute solution of sample kept in a thin capillary tube. The grazing-incidence measurement (GISAXS) employed here requires larger interfacial region that can be achieved by increasing the diameter of the tube containing the liquids. Increase in the diameter reduces measured intensity due to absorption of the x rays by the liquids. Keeping the thickness and absorption coefficients in mind, we prepared a teflon cylindrical cell of diameter 20 mm as shown in Fig. 1(a) and used 16 keV (wavelength, $\lambda = 0.0775$ nm) x rays of X21 beamline of National Synchrotron Light Source, Brookhaven National Laboratory (BNL), USA, for our experiments. Two windows were cut on diametrically opposite walls of the cell and Kapton sheets of 500 μm thickness are attached to allow x rays to go in and out of the cell for scattering measurement. The x-ray beam was first defined by a pair of slits [200 μm (vertical) $\times$500 μm (horizontal)] and then allowed to incident on toluene-water interface with an angle of 0.08°. We could not employ lower incident angle (note that critical angle for toluene-water interface is 0.03°) as larger portion of flat meniscus was not available in the cell. The diameter of the cylindrical cell was kept quite large to avoid scattering from meniscus that changes with the reaction. The strategy was a compromise between reducing the background scattering coming from the solution and having a flat enough interface to allow proper measurements.

The scattered intensity was collected using a two-dimensional (2D) MAR charge-coupled device (CCD) detector. The wave-vector transfer defined by the scattering angle 2θ for our experiment is $q=(4\pi/\lambda)\sin\theta$. The detector to sample distance was chosen to have q range from 0.6 to 6 nm^{-1} corresponding to length scale of 10.5 and 1.05 nm in real space. This length scale is ideal for studying the structure of aggregates of size 8 nm with the 1.2 nm gold-core

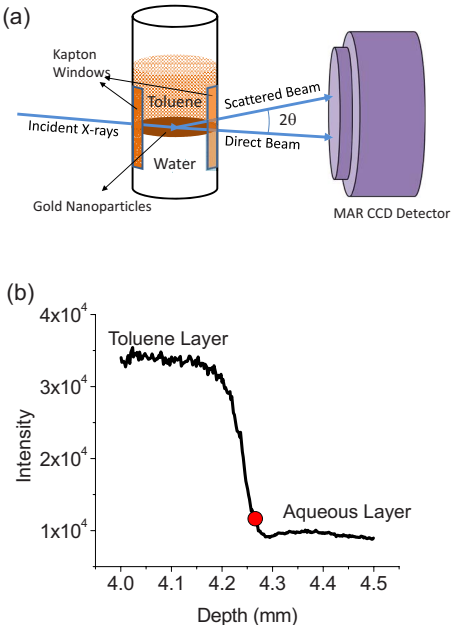

FIG. 1. (Color online) (a) Schematics of the experimental setup and small teflon cell used for the scattering experiments. (b) The direct beam intensity, passing through the cell containing the liquid, as a function of depth. The change in intensity is observed at the toluene-water interface. The filled circle is marked to locate the position of the interface from which all scattering data are collected.

nanoparticles as predicted in earlier measurements.[13,14] In our experiment, we blocked the direct beam with two types of beam stoppers. The large rectangular beam stopper (shown in right panel of Fig. 2) was used to collect the three-dimensional (3D) isotropic scattering at large **q** values while small rectangular beam stopper (shown in the left panel of Fig. 2) was used to collect the anisotropic scattering along q_z.

After the formation of the interface between the precursor solution in toluene and aqueous solution, we aligned the interface with the direct beam. In order to do that we collected the direct beam intensity passing through the cell with a point detector as the sample cell is scanned vertically. The interface could be located by a sharp change in the transmittance of the direct beam intensity [shown in Fig. 1(b)] due to the difference in absorption coefficients of toluene and water. By performing few initial measurements with the 2D detector during the film formation, we found that the scattering from the gold nanoparticles could be observed properly when beam is at a particular position [marked as filled circle in Fig. 1(b)] where the intensity of the direct beam was observed to be 90% of that from the toluene layer. We performed two sets of GISAXS measurements with the same settings but different sized beam stoppers to monitor the gold nanoparticle formation at the toluene-water interface as a function of time. We monitored the reaction for 350 min and the changes became slow beyond this reaction time.

III. RESULTS AND DISCUSSIONS

Representative data obtained with two different beam stoppers are shown in Fig. 2. Isotropic scattering from the

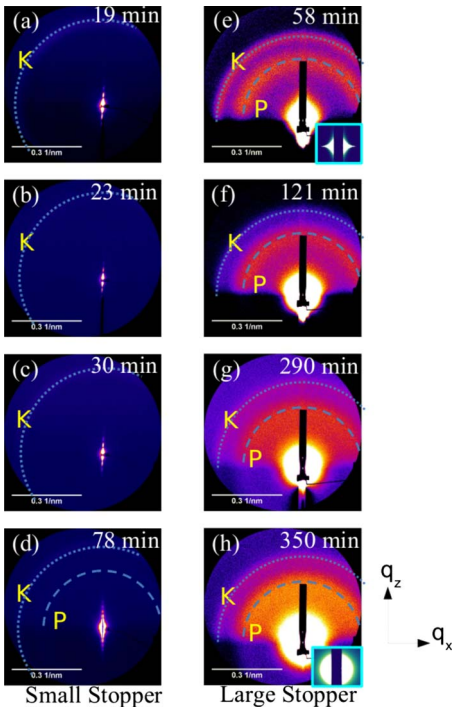

FIG. 2. (Color online) The two-dimensional scattering data collected by MAR CCD detector with small beam stopper after (a) 19 min, (b) 23 min, (c) 30 min, and (d) 78 min and with large beam stopper after (e) 58 min, (f) 121 min, (g) 290 min, and (h) 350 min after initiation of reaction. Insets of (e) and (h) are calculated scattering profiles from capillary-wave theory and fractal structure as discussed in the text.

Kapton windows produces an isotropic ring at $q=4$ nm^{-1} (marked as "K") in the data. Representative data collected with smaller beam stopper at the initial stage of the reaction in the left panel of Fig. 2 show intensity fringes along the q_z directions indicating the formation of a thin film at the interface. The period of these fringes decreased with reaction time indicating thickening of the film. We observed the formation of a circular ring (marked as "P") due to nanoparticle correlations at $q=2.8$ nm^{-1} after 30 min of the reaction. The data shown in Fig. 2(d) was collected after 78 min of reaction show this isotropic ring. In the second set of data with large beam stopper, we obtained better statistics for the correlation peak P to carry out detailed analysis [refer Figs. 2(e)–2(h)].

The formation of fringes along q_z at the initial stages of the reaction and the formation of isotropic ring at $q=2.8$ nm^{-1} at the later stage are the signatures of formation of the film of gold nanoparticles and its aggregation. In order to obtain quantitative information about the film thickness and the aggregation process, we analyzed different regions of the 2D data separately. There are three important regions of the data: (a) the low-q_z region with intensity fringes obtained with small beam stopper, (b) the peak at $q=2.8$ nm^{-1}, and (c) the q region from 0.4 to 1 nm^{-1} of the data collected with large beam stopper. The third region provides information about the nature of aggregation of the nanoparticles in the films at the toluene-water interface.

The scattering at low-q region is highly anisotropic at the initial stages of the reaction as evident from Figs. 2(a)–2(e).

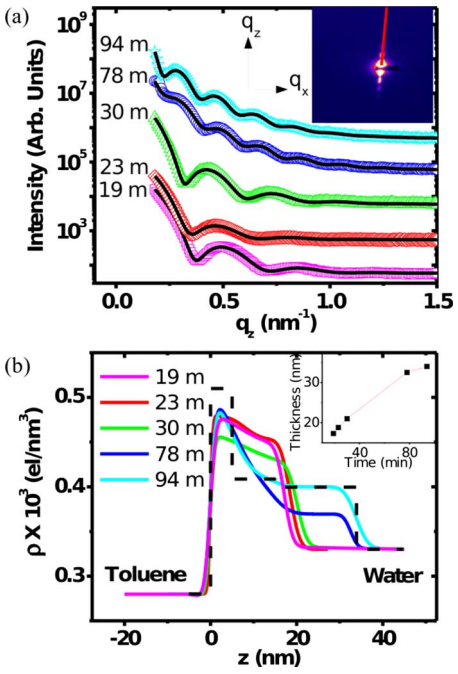

FIG. 3. (Color online) (a) The scattered intensities (symbols) as a function q_z, extracted from line profiles (integrated over small q_x values) on the two-dimensional data at different times. Inset: a two-dimensional data collected after 23 min to show the area marked as red line to extract the line profiles. The solid lines are fits generated from capillary-wave theory described in the text. (b) The electron-density profiles (solid lines) extracted by fitting the data shown in (a). The solid dashed line show a typical box model used for fitting described in the text. Inset: plot of thickness of the film as a function of time.

At later stages of reaction, the scattering in the low-q region became isotropic [refer Figs. 2(f)–2(h)].

Scattering intensity collected at the early stage of reaction from toluene-water interface [shown in Fig. 2(e)] with larger beam stopper, show the capillary-wave scattering at low-q values. For qualitative comparison, we have shown in the inset of Fig. 2(e), a two-dimensional plot of intensity calculated from capillary-wave theory.[23,24] The high background did not allow us to do the quantitative analysis[24] of line profile along q_x direction. As the reaction progressed, 3D scattering became apparent leading to isotropic scattering from gold particles both at low- and high-q values as shown Figs. 2(f)–2(h). In the inset of Fig. 2(h), we have shown the isotropic scattering intensity calculated from fractal structure of aggregates of gold nanoparticles that will be discussed later.

A. Low-q_z region

For the analysis of intensity fringes, we extracted the line profiles [refer Fig. 3(a)] as a function of q_z, integrated over small q_x values along the region marked as a line in the inset of Fig. 3(a). The profile at the initial stage of reaction was slightly tilted due to the tilting of the meniscus. As the reaction progressed the meniscus flattened due to the presence of

organic-shell-covered nanoparticles and became horizontal at later stages.

Fixed incidence angle (θ_i) scattering data at $q_x=0$ shown in Fig. 3(a) were analyzed using capillary-wave theory[23–25] assuming the film of gold nanoparticles to be conformal with the interface as

$$I(q) \propto \frac{R(q_z)q_z}{2k_o\sqrt{\pi}\sin\theta_i}\Gamma\left(\frac{1-\eta}{2}\right), \quad (1)$$

where $\eta=k_BTq_z^2/(2\pi\gamma)$ with k_B, T, and γ as Boltzmann constant, temperature, and interfacial tension. $k_o=2\pi/\lambda$ (λ being the wavelength of x rays) and Γ is the gamma function. The observed intensity fluctuations as a function of detector angle cannot be assumed as reflectivity pattern as incident and detector angles are unequal. Neglecting small variation in q_y in the measured range of data, we can obtain the Eq. (1) from the scattering expression of a liquid surface[23–25] where $R(q_z)$ is the specular reflectivity expression of a conformal thin film over liquid surface calculated using either Parratt formalism[26] or Born approximation.[27] We first obtained electron-density profiles (EDPs) of the film directly from the measured data shown in Fig. 3(a) using a model-independent inversion technique based on Born approximation.[27] The obtained EDP for each measured data was then approximated with simplest box model that mimic organic-shell-covered gold-core clusters, when convoluted with roughnesses at the edges of the boxes. The intensity profile was recalculated with this discrete box model by Parratt formalism[26] to reconfirm that the obtained data is represented well [refer Fig. 3(a)]. The simple box models thus obtained helped us to understand the aggregation process of the gold nanoparticles as a function of reaction time. A representative discrete box model for the EDP obtained for the data collected after 94 min of reaction is shown as solid dashed line and solid line with and without roughness convolution, respectively in Fig. 3(b). Roughness-convoluted electron-density profiles obtained for five representative data are shown in Fig. 3(b) as solid lines and corresponding fitted curves and measured data are shown in Fig. 3(a). In these calculations of Eq. (1) for fitting the data, we used a fixed value of interfacial tension value $\gamma=1.7$ mN/m as reported earlier,[13] for simplicity.

During the initial phase of the reaction, the electron-density profiles [shown in Fig. 3(b)] obtained from reflectivity fitting show two noticeable changes with time. First, there is an increase in the film thickness from 18 to 34 nm. Second, after 30 min, there is a modification of the electron-density profile with the appearance of a lower-density film near water. Three-dimensional scattering became prominent after the appearance of this low-density layer and isotropic scattering is observed [refer Fig. 2(d)]. The electron-density distributions shown in Fig. 3(b) clearly indicate that the nanoparticles aggregate more compactly away from the water surface giving rise to a decaying electron density toward water interface as the reaction progressed. We can hence infer accumulation of organic phase having less number of nanoparticle clusters near water interface. The position of the peak at $q=2.8$ nm^{-1} remain almost unchanged over the entire reaction time as we will discuss later. The layer of nanoparticle clusters of 40 nm thickness between the toluene and water layers reorganized itself as the reaction progressed. The formation of the ring around $q=2.8$ nm^{-1} clearly indicates that the scattering from the interfacial layer of 40 nm thickness is three dimensional in nature. A reduction in the rate of reaction is observed after about 60 min of reaction and this is apparent in the rate of increase in film thickness as shown in the inset of Fig. 3(b). This reduction in the rate of reaction is attributed to the formation of the low-density organic layer near water interface hindering the exchange of reactants between the toluene and water layers.

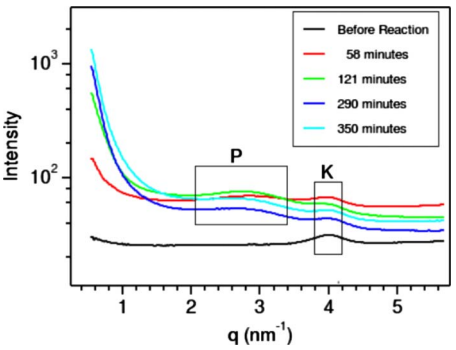

FIG. 4. (Color online) The azimuthally averaged data collected just before the reaction, which was considered as background and raw data collected at various the reaction times. It should be noted that the evolution of total intensity in this reflection geometry strongly depends on macroscopic morphology of the interfacial film and only relative intensities are important here. We confirmed by repeating the experiment several times that increase and decrease in overall intensity observed here varies from reaction to reaction.

B. Peak at $q=2.8$ nm^{-1}

In Fig. 4, we have shown azimuthally averaged raw data collected using large beam stopper along with a background data. The data collected from the interface before the initiation of the reaction was considered as the background. Only the upper half of the q space is used for this azimuthal averaging as scattering in lower half (through water) is much weaker. The presence of peaks due to nanoparticle-nanoparticle correlation at $q=2.8$ nm^{-1} are marked as P and peaks due to Kapton windows at $q=4.0$ nm^{-1} are marked as K in Fig. 4. The evolution of intensity in this reflection geometry strongly depends on macroscopic morphology of the interfacial film, entire interfacial layer within beam footprint cannot get illuminated as the film do not remain flat. We confirmed by repeating the experiment several times that increase and decrease in overall intensity due to onset of this roughness varies from reaction to reaction and for this set of data it was after 290 min of reaction. In the analysis of the data, we assumed that the scattering from the Kapton windows is independent of reaction time. The background data was scaled with proper factors to match the peak K of each data before carrying out background subtraction and same procedure was followed for all the data collected during a reaction.

The azimuthally averaged and background subtracted line profiles obtained around the peak [shown in Fig. 5(a)] were

analyzed with cluster model made of 13 nanoparticles.[13] In the absence of antivibration isolation, a large quantities of nanoparticles formed and the clusters formed by the nanoparticles start sharing the nanoparticles of each other. Due to this sharing there is reorganization of the nanoparticles and number of nanoparticles per cluster get reduced. We have, therefore, analyzed the peak assuming partial occupancy of the nanoparticles in the 13-member cluster. For incorporating partial occupancy, we summed over all possible clusters containing N_c nanoparticles ranging from 2 to 13 and write the azimuthally averaged scattering intensity as[28]

$$I(q) = K_o|F(q)|^2\left\{\sum_{N_c=2}^{13} P(N_c)\left(N_c + \sum_{i,j}^{N_c} \frac{\sin qd_{ij}}{qd_{ij}}\right)\right\}, \quad (2)$$

where K_o is a constant proportional to the number of scatterers and $F(q)$ is the form factor of the gold-core-organic-shell structure of individual gold nanoparticles with gold-core radius R_1 and organic capping thickness t_{org} with electron densities ρ_{core} and ρ_{org}, respectively. It is to be noted that in Eqs. (2) and (3), we have not considered effects of multiple scattering and neglected the effects of reflection and refraction in this high-q region. It is known[29] that the average number of interactions of x rays while passing a path Z through a film of nanoparticles of radius R_1 can be calculated as $N = 2\pi\rho Z\lambda^2\rho_{core}^2 r_e^2 R_1^4$. Here, ρ is the nanoparticle density in the film and r_e is the classical electron radius and we get maximum value of N about 0.01 for 50 nm film in grazing geometry. Multiple-scattering formalism can be avoided here as the value of N is much less than 0.1. In the expression of Eq. (2), $d_{i,j}$'s are the relative distances between ith and jth nanoparticles in a cluster. The coordinates (x,y,z) of the nanoparticles in a 13-member cluster used in our calculation are $\{0,0,0\}$ for the central nanoparticle, $\{\pm D,0,0\}$, $\{\pm D/2, \pm\sqrt{3}D/2,0\}$ for the six nanoparticles located in plane, $\{\pm D/2, D/(2\sqrt{3}), D\sqrt{2/3}\}$, $\{0, D(-\sqrt{3}+1/\sqrt{3})/2, D\sqrt{2/3}\}$ for three nanoparticles above the plane and $\{\pm D/2, -D/(2\sqrt{3}), -D\sqrt{2/3}\}$, $\{0, D(\sqrt{3}-1/\sqrt{3})/2, -D\sqrt{2/3}\}$ for the remaining three nanoparticles below the plane [shown in the inset of Fig. 5(a)]. $D=2(R_1+t_{org})$, is the separation between the two neighboring nanoparticles in a single cluster and $P(N_c)$ is the probability of getting a cluster with N_c number of nanoparticles. We assume the probability distribution of the cluster as $P(N_c)=(1-\tanh[(N_c-N_o)/\sigma])/2/P_{norm}$ to calculate the scattering intensity from Eq. (2). Here, σ is the width of the distribution, N_o is the average number of nanoparticles in the cluster having 13 cites, and P_{norm} is the normalization factor calculated by integrating the area under the curve of $P(N_c)$'s shown in Fig. 5(b). Increase in N_o increases the relative intensity of the peak and one cannot get the fitting of the peak shape and width without altering this parameter. The azimuthally averaged background subtracted data [refer Fig. 5(a)] was fitted with Eq. (2) keeping N_o, σ, D, and ρ_{org} as free parameters. The calculation using Eq. (2) was performed by assuming that the most probable state starts with 6+1 gold particles located in a plane (with $z=0$) and that 3 gold particles located above and below this plane further constitute the ideal cluster. The electron density of the gold core ρ_{core} and the organic shell ρ_{org} used are relative to the electron density of the toluene, i.e., 285 el/nm^3. We kept ρ_{core} fixed at 4000 el/nm^3 (bulk electron density of gold relative to that of toluene) in this analysis and the values of ρ_{org} obtained are shown in Table I along with the other parameters with corresponding error bars. We find that all the features of the correlation peak, namely, (1) peak position, (2) peak width, and (3) the difference between the intensities at the dip and at the peak, are correlated and highly dependent on N_o, ρ_{org}, and D. From Fig. 5(a), it is evident that with time the difference between the peak intensity and the dip (at $q=2$ nm^{-1}) decreased indicating a decrease in the contrast between the gold core and the organic shell. This observation is reflected in the increase in ρ_{org} values coming from our fitting. Also we found an increase in the width of the peak from 0.57 to 0.62 nm^{-1} by Gaussian fits of the peaks (not

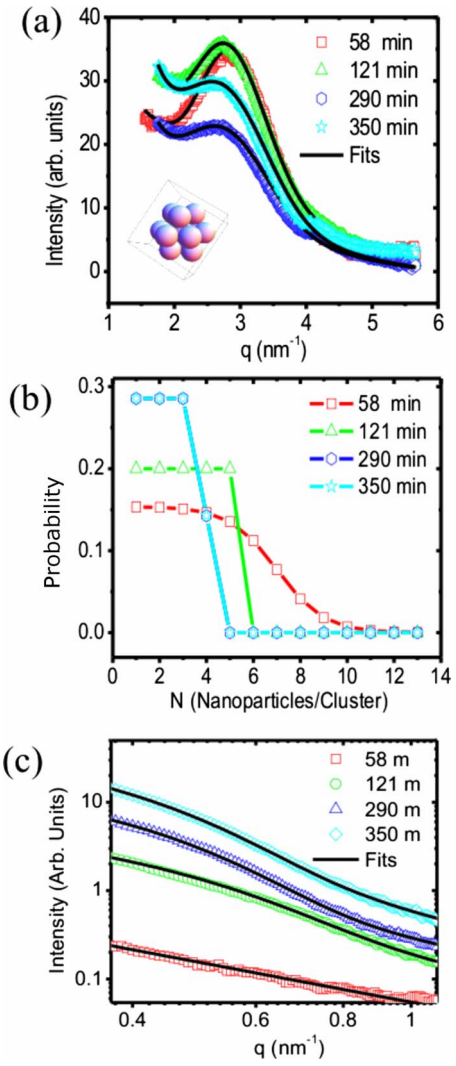

FIG. 5. (Color online) (a) The azimuthally averaged background subtracted data (symbols) for $q>1.5$ nm^{-1} collected at different times and the corresponding fits as discussed in the text. Inset: 3D schematics of the 13-member cluster. (b) The probability distribution of number of nanoparticles in the aggregates, used to fit the data in (a) as discussed in the text. (c) The background subtracted intensities (symbols) at different times for low-q values and the fits (solid lines) by fractal model as discussed in text. The data and the fit obtained for 350 min are multiplied by 2 for clarity.

TABLE I. Parameters obtained from fitting the peak due to separation of nanoparticles and the SAXS data for low-q values.

t (min)	N_o	σ	D (nm)	ρ_{org} (el/nm^3)	$K_o(\times 10^{-7})$	P_{norm}	G	R_2 (nm)	B	d_f
58	7	2.00	2.52 ± 0.004	78 ± 1	2.38	6.5	0.0	0.0	0.16	1.49 ± 0.02
121	5.5	0.01	2.50 ± 0.002	142 ± 2	6.36	5.0	2.75	4.00 ± 0.02	0.18	1.82 ± 0.08
290	4	0.01	2.44 ± 0.006	193 ± 4	5.16	3.5	13.21	4.80 ± 0.03	0.28	1.82 ± 0.04
350	4	0.01	2.42 ± 0.008	246 ± 5	6.50	3.5	31.56	4.90 ± 0.04	0.56	2.05 ± 0.08

shown here). This increase in peak width directly indicates the decrease in interparticle correlation of the nanoparticles in a cluster and is well reflected by the decrease in the value N_o. The values of D that determine the peak position showed a small decrease with time by 0.1 nm from 2.52 to 2.42 nm indicating compactification of the clusters. We also found the fits to be very sensitive to the core size of gold nanoparticles $(2R_1)$ which remained constant at 1.3 nm throughout the reaction. Apart form the initial value of $\sigma=2.0$ after 58 min of reaction, the value of σ is found to be negligible indicating sharp cutoff of the number of nanoparticles in the cluster around 4. In Fig. 5(b), we have shown the probability distribution of the clusters calculated from the fitted values of N_o and σ.

The azimuthally averaged and background subtracted peak and fitted curve obtained from Eq. (2) based on the cluster model having 13 gold nanoparticles provides a clear insight of the ordering of the nanoparticles. When the reaction was carried out on a antivibration table, the rate of formation of the nanoparticles was slow and there was sufficient time to form well-separated 13-member equilibrium structures.[13] In the absence of an antivibration table, a much thicker film is obtained at the interface due to macroscopic fluctuations. The value of N_o after 58 min of reaction showed that the clusters do not prefer to complete the 13-member equilibrium clusters in this situation. Rather they overlap with each other and the resultant clusters contain a smaller number of nanoparticles. This is reflected by the decrease in the value of N_o from 7 to 4 as the reaction progressed. Another important information from our analysis is that though there is a decrease in the number of nanoparticles per cluster with time, an increase in compactification of the structure of the clusters occurred. This compactification is reflected from the decrease in D value from 2.52 to 2.42 nm and increase in ρ_{org} value from 78 to 246 el/nm^3 relative to the electron density of toluene. The organic capping thickness around gold core, i.e., t_{org} calculated as $(D-2R_1)/2$ is found to be around 0.55 nm. The thickness of the organic capping reveals that the capping is a monolayer coverage of left over organic precursor molecules of size about 0.5 nm.[30]

C. q region from 0.4 to 1 nm^{-1}

The obtained final value of N_o as 4 with low σ clearly indicated formation of two-dimensional clusters of gold nanoparticles as first seven cites of 13 clusters model are assumed to be in a plane here. On the other hand, in the beginning of reaction, we get a value of N_o as 7 and high value of σ—this indicate "partial occupancy" of a three-dimensional cluster having 13 cites. We carried out fractal analysis of low-q intensity profile to understand the effect of such fractional occupancy of cluster in altering the fractal dimensionality and the effective sizes of such clusters.

Figure 5(c) shows the background subtracted scattering intensities at small q values obtained from the interface at different times of the reaction. The presence of gold nanoparticles at the interface increased the scattering intensity at all the q values. Though the length scales probed by our present measurements is just about the size of the clusters, the extracted fractional occupancy motivated us to analyze the data with a fractal structure model at these length scales. We fitted the background subtracted data [shown as solid lines in Fig. 5(c)] with global fitting function for fractal structures[19,20] as

$$I(q) = G \exp[-q^2R_2^2/3] + Bq^{-d_f}. \quad (3)$$

The first term is the Guinier term and depends on cluster size $2R_2$ and the second term is due to fractal structure of the cluster with fractal dimension d_f. Here, G is Guinier prefactor which depends on number density of nanoparticles and B, the scaling prefactor, signifies the strength of power-law scattering arising from the fractal structure.[21,22] The values of parameters obtained after fitting are enlisted in Table I.

The 2D data collected after 58 min of reaction at small q values with the large beam stopper is highly anisotropic due to capillary-wave scattering as shown in Fig. 2(e). Due to this anisotropy, the values of R_2 and d_f obtained from the fitting of the low-q data for 58 min are questionable. On the contrary, the low-q scattering data for the longer durations of reaction, i.e., 121 min onward are isotropic and can be considered as three-dimensional scattering from clusters of nanoparticles. The values of R_2 and fractal dimension d_f show that cluster size increased with reaction time from 8 to 10 nm and the fractal dimension 1.82 to 2.05. It is known that the fractal dimension of aggregates formed by cluster-cluster aggregation process is $d_f=1.75$. The value $d_f=1.82$ found at early reaction times is close to this value. As the reaction progressed, higher values of d_f are obtained along with an increase in the values of G and B. The increase in the values of G and B directly gives a direct indication of the increase in the density of nanoparticles or their compactification. Such an increase in fractal dimension due to compactification process has been observed earlier.[16] It is to be noted here that a fractal dimension 2 would be consistent with disklike aggregates.[20]

IV. CONCLUSIONS

In conclusion, we have studied the aggregation process of gold nanoparticles formed at the toluene-water interface using GISAXS. The measurements provide us direct evidence for the formation of 1.3 nm diameter gold nanoparticles with a particle-particle distance of about 2.5 nm. We demonstrated that in the absence of an antivibration, the nanoparticles aggregate to form thick interfacial films where the diameter and separation between nanoparticles remained almost unchanged. The monolayer of 13-member cluster[13] formed in the interfacial reaction with the use of antivibration isolation exhibit fractional occupancy as the film thickness increases when the reaction is carried out without the antivibration isolation.

By combining both the results of fractal analysis of low-q scattering data and multiple cluster analysis of the peak, we can model the growth of the clusters as follows. The reaction at the microscopic level produces gold nanoparticles of sizes around 1.3 nm which aggregate to form incomplete clusters. The clusters are incomplete in the sense that they do not have the full outer shell and the cites are fractionally occupied. The incomplete clusters aggregate to form fractal structures and then reorganize to form compact structures with decrease in interparticle separation. The increase in fractal dimension from 1.82 to 2.05 is due to the reorganization and compactification of the clusters in the film in the course of the reaction. The compact portion of the film moves toward toluene layer leaving behind an organic-rich layer near water interface.

M.K. Bera and M.K. Sanyal acknowledge Department of Science and Technology, India for full financial assistance in performing the experiments at BNL, USA. M.K. Bera also acknowledges CSIR, India, for funding and support. Use of the National Synchrotron Light Source, Brookhaven National Laboratory, was supported by the U.S. Department of Energy, Office of Science, Office of Basic Energy Sciences, under Contract No. DE-AC02-98CH10886. M.K. Sanyal acknowledges Universit du Maine for financial support during his visit in Le Mans where initial theoretical ideas were generated.

[1] J. M. Wessels, H.-G. Nothofer, W. E. Ford, F. v. Wrochem, F. Scholz, T. Vossmeyer, A. Schroedter, H. Weller, and A. Yasuda, J. Am. Chem. Soc. **126**, 3349 (2004).
[2] S. Pal, M. K. Sanyal, N. S. John, and G. U. Kulkarni, Phys. Rev. B **71**, 121404(R) (2005).
[3] P. Dutta, S. Pal, M. S. Seehra, M. Anand, and C. B. Roberts, Appl. Phys. Lett. **90**, 213102 (2007).
[4] P. Crespo, R. Litrań, T. C. Rojas, M. Multigner, J. M. de la Fuente, J. C. Sańchez-López, M. A. Garcia, A. Hernando, S. Penadeś, and A. Fernańdez, Phys. Rev. Lett. **93**, 087204 (2004).
[5] Y. Yamamoto, T. Miura, M. Suzuki, N. Kawamura, H. Miyagawa, T. Nakamura, K. Kobayashi, T. Teranishi, and H. Hori, Phys. Rev. Lett. **93**, 116801 (2004).
[6] W. Rechberger, A. Hohenau, A. Leitner, J. R. Krenn, B. Lamprecht, and F. R. Aussenegg, Opt. Commun. **220**, 137 (2003).
[7] M. A. Garcia, J. de la Venta, P. Crespo, J. LLopis, S. Penades, A. Fernandez, and A. Hernando, Phys. Rev. B **72**, 241403(R) (2005).
[8] M. D. Hughes, Y.-J. Xu, P. Jenkins, P. McMorn, P. Landon, D. I. Enache, A. F. Carley, G. A. Attard, G. J. Hutchings, F. King, E. Hugh Stitt, P. Johnston, K. Griffin, and C. J. Kiely, Nature (London) **437**, 1132 (2005).
[9] M. Turner, V. B. Golovko, O. P. H. Vaughan, P. Abdulkin, A. Berenguer-Murcia, M. S. Tikhov, B. F. G. Johnson, and R. M. Lambert, Nature (London) **454**, 981 (2008).
[10] M.-C. Daniel and D. Astruc, Chem. Rev. **104**, 293 (2004).
[11] C. N. R. Rao, G. U. Kulkarni, P. J. Thomas, V. V. Agrawal, and P. Saravanan, J. Phys. Chem. B **107**, 7391 (2003).
[12] C. N. R. Rao and K. P. Kalyanikutty, Acc. Chem. Res. **41**, 489 (2008).
[13] M. K. Sanyal, V. V. Agrawal, M. K. Bera, K. P. Kalyanikutty, J. Daillant, C. Blot, S. Kubowicz, O. Konovalov, and C. N. R. Rao, J. Phys. Chem. C **112**, 1739 (2008).
[14] M. K. Bera, M. K. Sanyal, R. Banerjee, K. P. Kalyanikutty, and C. N. R. Rao, Chem. Phys. Lett. **461**, 97 (2008).
[15] I. Benjamin, Chem. Rev. **96**, 1449 (1996).
[16] D. W. Schaefer, J. E. Martin, P. Wiltzius, and D. S. Cannell, Phys. Rev. Lett. **52**, 2371 (1984).
[17] P. Dimon, S. K. Sinha, D. A. Weitz, C. R. Safinya, G. S. Smith, W. A. Varady, and H. M. Lindsay, Phys. Rev. Lett. **57**, 595 (1986).
[18] A. K. Boal, F. Ilhan, J. E. DeRouchey, T. Thurn-Albrecht, T. P. Russell, and V. M. Rotello, Nature (London) **404**, 746 (2000).
[19] H. K. Kammler, G. Beaucage, D. J. Kohls, N. Agashe, and J. Ilavsky, J. Appl. Phys. **97**, 054309 (2005).
[20] G. Beaucage, Phys. Rev. E **70**, 031401 (2004).
[21] G. Beaucage, J. Appl. Crystallogr. **29**, 134 (1996).
[22] J. Liao, Y. Zhang, W. Yu, L. Xu, C. Ge, J. Liu, and N. Gua, Colloids Surf., A **223**, 177 (2003).
[23] S. K. Sinha, E. B. Sirota, S. Garoff, and H. B. Stanley, Phys. Rev. B **38**, 2297 (1988).
[24] M. K. Sanyal, S. K. Sinha, K. G. Huang, and B. M. Ocko, Phys. Rev. Lett. **66**, 628 (1991).
[25] J. K. Basu and M. K. Sanyal, Phys. Rep. **363**, 1 (2002).
[26] L. G. Parratt, Phys. Rev. **95**, 359 (1954).
[27] M. K. Sanyal, S. Hazra, J. K. Basu, and A. Datta, Phys. Rev. B **58**, R4258 (1998).
[28] J. Als-Nielsen and D. MacMorrow, *Elements of Modern X-Ray Physics* (Wiley, England, 2001).
[29] S. Mazumder, B. Jayaswal, and A. Sequeira, Physica B **241-243**, 1222 (1997).
[30] R. E. Benfield, A. Filipponi, D. T. Bowron, R. J. Newport, and S. J. Gurman, J. Phys.: Condens. Matter **6**, 8429 (1994).